UV absorption spectrum of the C2 Criegee intermediate CH3CHOO

Mica C. Smith, Wei-Lun Ting, Chun-Hung Chang, Kaito Takahashi, Kristie A. Boering, and Jim Jr-Min Lin

Citation: The Journal of Chemical Physics **141**, 074302 (2014); doi: 10.1063/1.4892582
View online: http://dx.doi.org/10.1063/1.4892582
View Table of Contents: http://scitation.aip.org/content/aip/journal/jcp/141/7?ver=pdfcov
Published by the AIP Publishing

UV absorption spectrum of the C2 Criegee intermediate CH_3CHOO

Mica C. Smith,[1,2] Wei-Lun Ting,[2] Chun-Hung Chang,[2] Kaito Takahashi,[2]
Kristie A. Boering,[1,3] and Jim Jr-Min Lin[2,4,5,a)]
[1]*Department of Chemistry, University of California, Berkeley, Berkeley, California 94720, USA*
[2]*Institute of Atomic and Molecular Sciences, Academia Sinica, Taipei 10617, Taiwan*
[3]*Department of Earth and Planetary Science, University of California, Berkeley, Berkeley, California 94720, USA*
[4]*Department of Chemistry, National Taiwan University, Taipei 10617, Taiwan*
[5]*Department of Applied Chemistry, National Chiao Tung University, Hsinchu 30010, Taiwan*

(Received 19 June 2014; accepted 25 July 2014; published online 15 August 2014)

The UV spectrum of CH_3CHOO was measured by transient absorption in a flow cell at 295 K. The absolute absorption cross sections of CH_3CHOO were measured by laser depletion in a molecular beam to be $(1.06 \pm 0.09) \times 10^{-17}$ cm^2 molecule^{-1} at 308 nm and $(9.7 \pm 0.6) \times 10^{-18}$ cm^2 molecule^{-1} at 352 nm. After scaling the UV spectrum of CH_3CHOO to the absolute cross section at 308 nm, the peak UV cross section is $(1.27 \pm 0.11) \times 10^{-17}$ cm^2 molecule^{-1} at 328 nm. Compared to the simplest Criegee intermediate CH_2OO, the UV absorption band of CH_3CHOO is similar in intensity but blue shifted by 14 nm, resulting in a 20% slower photolysis rate estimated for CH_3CHOO in the atmosphere. © *2014 AIP Publishing LLC*. [http://dx.doi.org/10.1063/1.4892582]

INTRODUCTION

Carbonyl oxides, or Criegee intermediates, have been studied extensively with the aim of understanding their chemical properties and their role as oxidizers in the troposphere.[1,2] Criegee proposed the formation of such intermediates in the reaction of ozone with unsaturated hydrocarbons.[3,4] An example is shown in (R1) for ethene. The carbonyl oxide formed (e.g., CH_2OO) may subsequently decompose, undergo photolysis, or react with other species. Because the formation of Criegee intermediates during ozone-alkene reactions is much slower than their decomposition,[5,6] these species typically have low steady-state concentrations, which have hindered efforts to directly detect Criegee intermediates in the laboratory until recently,[7]

$$CH_2 = CH_2 + O_3 \rightarrow CH_2OO + CH_2O \rightarrow \text{products}. \quad \text{(R1)}$$

The simplest Criegee intermediate, CH_2OO, was directly observed by Welz *et al.*[8] using tunable vacuum UV photoionization mass spectrometry (PIMS), a sensitive technique that allowed separation of CH_2OO from its various isomers on the basis of ionization energies. Remarkably, their work introduced an efficient method for producing CH_2OO and other Criegee intermediates, by preparing CH_2I_2 (or a corresponding diiodoalkane) in O_2 and irradiating the mixture with UV light. CH_2OO is then produced by the reaction of the resulting CH_2I with O_2. Subsequent studies have adapted this synthesis scheme to characterize vibrational,[9] rotational,[10] and electronic states[11–14] of CH_2OO, as well as its reactivity with atmospheric species such as SO_2, NO_2, and volatile organic compounds.[8,15–20] Notably, an unexpectedly large rate coefficient was determined for the reaction of CH_2OO with SO_2.[8] This result could dramatically alter estimates of sulfuric acid concentrations and aerosol formation rates in the atmosphere.[21]

Most work has focused on the simplest Criegee intermediate CH_2OO. Only a handful of studies have investigated other carbonyl oxides such as CH_3CHOO, the "next simplest" Criegee intermediate. Taatjes *et al.*[22] probed the *syn*- and *anti*-conformers of CH_3CHOO with PIMS and estimated the relative thermal population of the *syn*-conformer over the *anti*-conformer to be 90:10 at 298 K, assuming similar photoionization cross sections for both conformers. They also determined conformer-specific rate constants for reaction with SO_2 and H_2O.[22] Beames *et al.* measured the UV absorption spectrum of CH_3CHOO by laser depletion of the ground electronic state of CH_3CHOO in a jet-cooled molecular beam, which was detected with PIMS at 10.5 eV.[23]

Direct measurement of the UV absorption spectrum of CH_3CHOO has not been reported. Furthermore, considerable discrepancies in the reported UV spectra of CH_2OO[11–13] suggest that additional studies may also be necessary for CH_3CHOO. In this work, the UV absorption spectrum of CH_3CHOO is measured by transient absorption spectroscopy, and is scaled to the absolute absorption cross section at 308 nm measured by laser depletion in a molecular beam.

EXPERIMENTAL AND THEORETICAL METHODS

Transient absorption spectroscopy

The transient absorption measurements of CH_3CHOO were carried out in a flow apparatus, modified slightly from previous descriptions.[13,24] For the CH_3CHOO absorption experiments, a mixture of O_2 and N_2 was bubbled through liquid CH_3CHI_2 (Aldrich, ≥98.0%). The CH_3CHI_2 liquid was slightly heated (311 K) to ensure saturation of its vapor above the liquid, resulting in a stable concentration of CH_3CHI_2 in the gas flow. For SO_2 scavenging experiments, SO_2 (99.98%)

a)Email: jimlin@gate.sinica.edu.tw.

was also introduced from a cylinder maintained at 273 K to achieve a low vapor pressure for easier flow control. The mixing ratio of each gas (CH_3CHI_2, O_2, N_2, and SO_2) was controlled by four mass flow controllers (Brooks Instruments, 5850E). A fifth mass flow controller was used to maintain a small flow of the N_2/O_2 carrier gas (1%–2% of the total N_2/O_2 flow rate) near the photolysis cell windows to avoid contamination. All gases were mixed in Teflon tubes and passed through a smaller cell (201 mm long) upstream of the photolysis cell. The absorption of CH_3CHI_2 and SO_2 in this small cell was monitored continuously throughout the experiment with a D_2 lamp (Ocean Optics, D-2000) and a spectrometer (Ocean Optics, USB2000+UV-VIS-ES).

Transient absorption in the photolysis cell (750 mm long, 20 mm inner diameter) was detected with a continuous light source (Energetiq, EQ-99) and a gated iCCD spectrometer (Spectrometer: Andor SR303i; iCCD: Andor iStar DH320T-18F-E3). The wavelength scale of the spectrometer was calibrated with the emission spectrum from a mercury lamp (1.5 nm resolution, calibration accuracy 0.25 nm) before each experiment. The pressure and flow rate in the photolysis cell were controlled with the mass flow controllers and an outlet valve to a mechanical pump. A linear flow velocity faster than 0.8 m/s was maintained to allow complete refreshment of gases between laser pulses (1 Hz repetition rate).

CH_3CHOO was produced from photolysis of CH_3CHI_2 by a 248 nm KrF excimer laser (Coherent Compex Pro 205 F) and subsequent reaction of CH_3CHI with O_2. The change in absorption by CH_3CHOO and other species was measured at a series of delay times (16 or 18 delay times total, ranging from 1 to 484 μs) between the laser pulse and the center of the iCCD spectrometer gate opening (gate width 1 μs). In addition, one reference spectrum was recorded before the photolysis laser pulse. The delay sequence was controlled automatically by a program written in Andor Basic within the iCCD spectrometer data acquisition software (Andor Solis). Signal at each delay time was accumulated over at least 120 laser pulses for each set of experimental conditions to improve the signal-to-noise ratio.

Absolute cross section measured by photodepletion in a molecular beam

The absolute absorption cross sections of CH_3CHOO at 308 and 352 nm were determined by laser depletion of CH_3CHOO in a molecular beam. A mixture of 20% O_2 in Ar was bubbled through liquid CH_3CHI_2. The $CH_3CHI_2/O_2/Ar$ mixture flowed through a pulsed valve operating at 50 Hz (with a typical backing pressure of 30 psia) and entered a SiO_2 capillary (1 mm inner diameter, 20 mm length) attached to the pulsed valve nozzle. An excimer laser (XeCl or XeF, Lambda Physik, LPX-210i) with a pulse rate of 50 Hz (308 nm for the 352 nm depletion measurements, 352 nm for the 308 nm measurements) was used to photolyze CH_3CHI_2 in the SiO_2 capillary. The resulting CH_3CHI in the capillary reacted with O_2 to form CH_3CHOO. The mixture gas then expanded at the exit of the SiO_2 capillary. After passing through a skimmer (4 mm diameter) 45 cm downstream of the SiO_2 capillary, the molecular beam was further defined with a slit (0.5 mm height, 4 mm width).

The molecular beam signal was detected with a mass spectrometer located 75 cm downstream of the SiO_2 capillary. CH_3CHOO molecules were ionized by electron impact at 45 eV, and the ions traveled through a quadrupole mass filter to a Daly detector. Arrival time profiles of CH_3CHOO (at $m/z = 60$, $C_2H_4O_2^+$) were recorded using a multichannel scaler (Ortec, Turbo-MCS).

Another excimer laser beam operating at 25 Hz (at either 352 nm or 308 nm) intersected the CH_3CHOO molecular beam directly after it passed the defining slit at a point 25 cm upstream of the mass spectrometer, resulting in depletion of the signal at $m/z = 60$. The laser beam was attenuated homogeneously by a variable attenuator (Laseroptik, IVA351nm or IVA308nm) to the desired pulse energy, which was measured with a power meter (Gentec-EO, UP25N + Solo 2 controller).

Under the molecular beam conditions in these experiments, the photodepletion signal can be related to the absorption cross section σ, the photodissociation quantum yield ϕ, and the laser fluence I using Eq. (1), where N_0 and N are the numbers of molecules before and after laser irradiation,

$$\frac{N}{N_0} = e^{-I\sigma\phi}, \quad \frac{\Delta N}{N_0} = \frac{N_0 - N}{N_0} = 1 - e^{-I\sigma\phi}. \tag{1}$$

Absorption at the wavelengths studied here excites CH_3CHOO and CH_3CHI_2 to repulsive states or states higher than their dissociation thresholds,[23] resulting in rapid and complete dissociation ($\phi = 1$). Because of inhomogeneity in the laser beam profile, however, the absolute laser fluence I may be difficult to quantify with sufficient accuracy to yield accurate cross sections σ for CH_3CHOO using Eq. (1). Two additional methods of determining absolute CH_3CHOO cross sections were therefore used.

First, in addition to measuring the depletion of CH_3CHOO, the relative depletion of CH_3CHI_2 at 308 nm was measured in the molecular beam. By analyzing the experimental data using Eq. (1), the value of $I\sigma$ was obtained for both CH_3CHOO and CH_3CHI_2, assuming $\phi = 1$. From this, the ratio $\sigma(CH_3CHOO)/\sigma(CH_3CHI_2)$ can then be deduced. As discussed below, if $\sigma(CH_3CHI_2)$ is known and reliable, the absolute value of $\sigma(CH_3CHOO)$ can then be obtained.

Second, a method was developed to estimate the absolute fluence of the excimer laser beam. The profile of the laser beam was recorded using a laser beam profiling digital camera (WinCamD, model UCD23, 8.8 mm × 6.6 mm image area, 6.45 μm × 6.45 μm pixel area, 14-bit ADC) and DataRay imaging software. A rectangular slit (2 mm high, 19 mm wide) in the laser beam path, 15 mm ahead of the laser beam-molecular beam crossing point, removed the "wings" of the laser beam vertical profile so that only the most intense and uniform portion of the laser beam was used. Using the measured laser pulse energy and the intensity profile, the absolute laser fluence can be deduced. See the supplementary material[25] for further experimental details.

Theoretical calculations

Detection of the Criegee intermediate in the experiments described above may be subject to interference from isomers of CH_3CHOO. To investigate the possible isomers of CH_3CHOO, geometry optimization was performed using density functional theory with Becke's three parameter hybrid functional (B3LYP),[26,27] coupled cluster singles and doubles with perturbative triples (CCSD(T)),[28–31] and multireference complete active space self-consistent field (MC CASSCF) methods.[32,33] The two single reference methods were employed using Dunning's aug-cc-pVTZ basis set, and the CASSCF calculation was performed using the aug-cc-pVDZ basis set.[34,35] For the CASSCF method, all core electrons and the 2*s* electrons on carbon and oxygen were frozen. Furthermore, due to computational limitations, two high energy orbitals were removed from the full valence active space, thus giving an active space of 16 electrons in 14 orbitals. Additional CASSCF optimization was performed using an active space of 10 electrons in 10 orbitals, which corresponds to the 5 important bonds for the description of the different isomers of CH_3CHOO.

The single reference methods yielded 7 stable molecular minima and 2 OH radical complexes, while one extra molecular minimum was obtained using the CASSCF method. For B3LYP and CASSCF(10,10), frequency calculations were performed to confirm that the calculated geometries are minima. Using these optimized geometries, the electronic transition energies and oscillator strengths were calculated for the first four excited states by performing single-point CCSD equation-of-motion (CCSD-EOM)[36–38] calculations with the aug-cc-pVTZ basis set. The B3LYP calculations were performed using the Gaussian 09 program[39] while all other calculations were performed using the MOLPRO program.[40]

RESULTS AND DISCUSSION

Figure 1 (top) shows examples of transient absorption measured at different photolysis delay times. Depletion of the broad CH_3CHI_2 absorption due to photolysis in (R2) below results in the negative absorbance peaked near 290 nm, and absorption of CH_3CHOO (the peak labeled as band A) appears in the first few μs due to (R3) below and decreases as the delay time is increased. Formation of IO is likely due to (R4), and its distinct vibrational peaks at 412, 420, 428, and 436 nm appear at longer delay times. Absorption spectra[41] for CH_3CHI_2 and IO, along with further details of data analysis, are available in the supplementary material,[25]

$$CH_3CHI_2 + h\nu \rightarrow CH_3CHI + I, \quad \text{(R2)}$$

$$CH_3CHI + O_2 \rightarrow CH_3CHOO + I, \quad \text{(R3)}$$

$$CH_3CHOO + I \rightarrow CH_3CHO + IO, \quad \text{(R4)}$$

$$CH_3CHOO + SO_2 \rightarrow \text{products}, \quad \text{(R5)}$$

$$CH_3CHOO + CH_3CHOO \rightarrow \text{products}. \quad \text{(R6)}$$

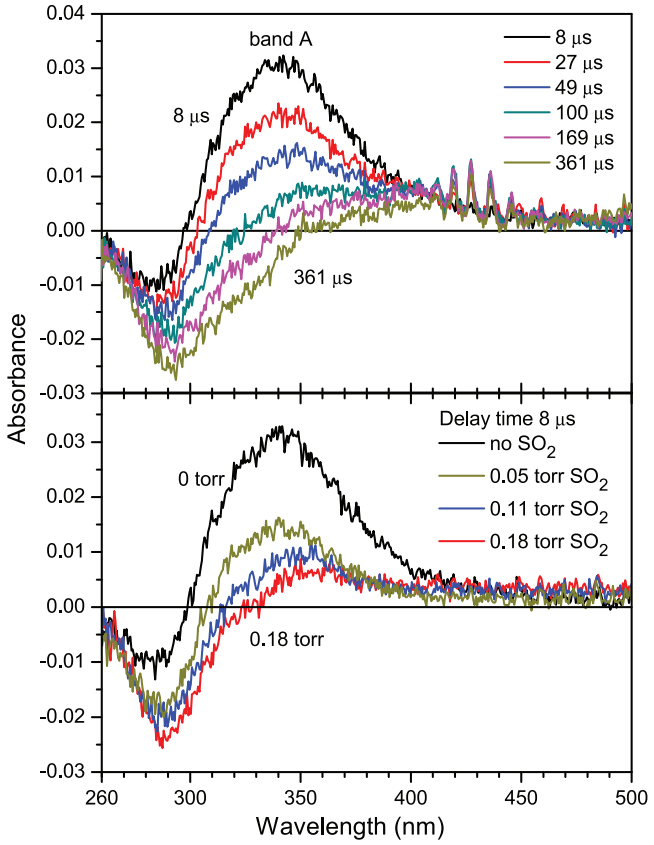

FIG. 1. (Top) Examples of transient absorbance traces probed at different delay times after the photolysis pulse, with no SO_2 present. Depletion of CH_3CHI_2 results in the negative absorbance peaked near 290 nm. Formation of IO gives rise to distinct peaks at 412, 420, 428, and 436 nm at longer delay times. Absorption of CH_3CHOO, with peak labeled band A, decreases with increasing delay time. Estimated number densities in the cell are $[CH_3CHI_2]_0 = 1.2 \times 10^{16}$ cm^{-3}, $[O_2]_0 = 9.7 \times 10^{17}$ cm^{-3}, total number density (N_2 balance) 2.1×10^{18} cm^{-3}. (Bottom) Examples of absorbance traces at a delay time of 8 μs at different SO_2 concentrations. $[CH_3CHI_2]_0 = 1.3 \times 10^{16}$ cm^{-3}, $[O_2]_0 = 1.0 \times 10^{18}$ cm^{-3}, total number density 2.1×10^{18} cm^{-3}.

The fast rate of (R5) ($2.4–6.7 \times 10^{-11}$ cm^3 molecule^{-1} s^{-1} reported by Taatjes *et al.*[22]) allows SO_2 to be used as an efficient scavenger for CH_3CHOO. Figure 1 (bottom) shows absorbance traces for different concentrations of SO_2 scavenger. The rapid depletion in absorbance upon addition of SO_2 is expected to originate solely from CH_3CHOO depletion (since the absorption change due to other species consumed or produced, such as SO_2, CH_3CHO, and SO_3, is much weaker). When all experimental conditions except the SO_2 concentrations are kept constant, subtracting the absorbance in the presence of SO_2 from the absorbance without SO_2 yields an absorption spectrum containing contributions from CH_3CHOO and SO_2 at a 1:1 ratio.[13] After scaling the UV absorption spectrum to the absolute cross sections obtained by laser depletion (discussed below), the contribution of SO_2 absorption to the spectrum can be easily removed.

As shown in the supplementary material,[25] the SO_2 scavenging experiments allowed us to measure the decay rate of CH_3CHOO in the presence of SO_2 under pseudo first-order conditions. We determined the rate constant for (R5)

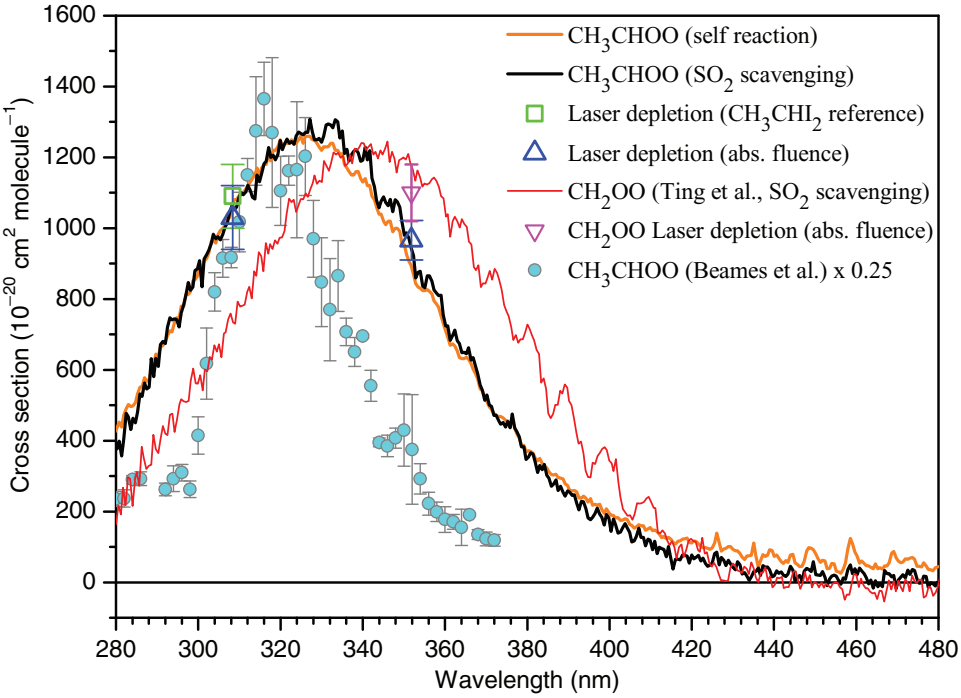

FIG. 2. Comparison of CH_3CHOO and CH_2OO absorption spectra. Black and orange lines are the CH_3CHOO spectra obtained here using the SO_2 scavenger and self-reaction methods. Square and triangle symbols indicate cross section measurements from laser depletion. Blue filled circles are the CH_3CHOO absorption measurements of Beames *et al.*,[23] scaled by a factor of 0.25 to roughly match our absolute absorption cross section at 308 nm. The thin red line is the spectrum of CH_2OO measured by Ting *et al.*[13]

to be $(2.0 \pm 0.3) \times 10^{-11}$ cm^3 molecule^{-1} s^{-1}, which agrees with a value of $(2.4 \pm 0.3) \times 10^{-11}$ cm^3 molecule^{-1} s^{-1} reported for the dominant *syn*-conformer of CH_3CHOO.[22] Under our experimental conditions, we did not observe the kinetics of the *anti*-conformer, which is reasonable if its thermal population is only 10%.[22] The *anti*-conformer was reported to react with SO_2 at a faster rate of $(6.7 \pm 1.0) \times 10^{-11}$ cm^3 molecule^{-1} s^{-1}.[22]

Without SO_2 in the photolysis cell, decay of CH_3CHOO is due primarily to (R6), the self-reaction of the Criegee intermediate, and to (R4), the reaction of CH_3CHOO with I atoms. Because (i) CH_3CHI is consumed by excess O_2 within the first few μs, (ii) CH_3CHOO is relatively short-lived in comparison with CH_3CHI_2 and IO, and (iii) the shapes of the CH_3CHI_2 and IO spectra are quite distinct, the contributions of CH_3CHI_2 and IO to the absorbance can be easily subtracted. The resulting spectrum is consistent with the spectrum obtained using SO_2 scavenger (see Figure 2), although slight discrepancies at wavelengths longer than 400 nm suggest contributions from other absorbing species (possibly CH_3CHIOO, an adduct of CH_3CHI and O_2). The SO_2 scavenging method used in this work to extract the CH_3CHOO spectrum provides species selectivity based on the chemical reactivity of CH_3CHOO. The "self-reaction" method has somewhat lower selectivity. Hence, the small discrepancies between the SO_2-scavenging spectrum and the self-reaction spectrum in Figure 2 likely originate from contaminants that have weaker absorption.

While the absorbance due to CH_3CHOO can be extracted from the transient absorption, it is difficult to know the absolute number density of CH_3CHOO in the photolysis cell. Therefore, to convert the spectrum of CH_3CHOO to absorption cross sections, the absolute cross sections at 308 nm and 352 nm were measured by mass spectrometric detection of the laser depletion of CH_3CHOO in a molecular beam. This method has been used previously to selectively detect species with short lifetimes and at low concentrations.[13,42,43] Figure 3 (top solid symbols) shows the CH_3CHOO depletion signal ($\Delta N/N_0$) at 308 nm at a variety of laser pulse energies and the fit to Eq. (1). The good fit indicates that a single species is being measured (or multiple species that have similar cross sections). At high laser energy the CH_3CHOO signal approaches 100% depletion, consistent with $\phi = 1$. The relative depletion of CH_3CHI_2 was also measured under similar conditions, shown in Figure 3 (top open symbols) with the fit to Eq. (1). Saturation of the CH_3CHOO depletion signal occurs at a lower laser pulse energy than that for CH_3CHI_2, indicating the cross section of CH_3CHOO is larger.

Because the temperature in a molecular beam (e.g., $T_{rot} \approx 10$ K) is much lower than room temperature, we must consider the effect of temperature on the absorption cross section. 308 nm is near the peak of the CH_3CHI_2 UV absorption band[41] and is therefore likely to have a negligible temperature dependence, as observed for CH_2I_2.[41,44] Assuming the low temperature cross section at 308 nm is the same as that at 298 K for CH_3CHI_2, we may use the laser depletion of CH_3CHI_2 to calibrate the laser fluence. In other words, since we know the relative laser fluence for both the CH_3CHOO and CH_3CHI_2 experiments, we can deduce the cross section ratio $\sigma(CH_3CHOO)/\sigma(CH_3CHI_2)$, and, subsequently, $\sigma(CH_3CHOO)$ based on the literature value of $\sigma(CH_3CHI_2)$ at 298 K.[41]

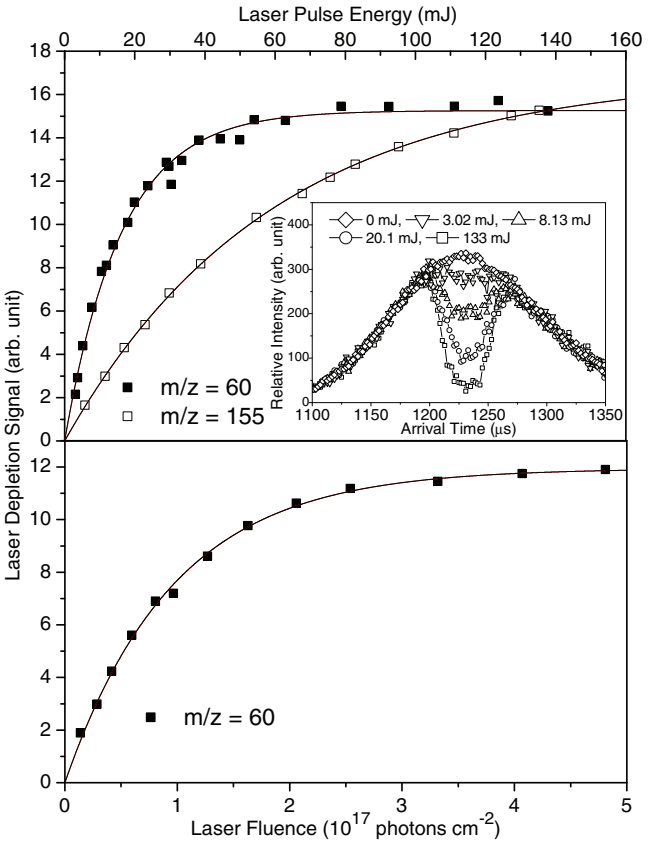

FIG. 3. (Top) Saturation curves for laser depletion of CH_3CHOO ($m/z = 60$) and CH_3CHI_2 ($m/z = 155$, CH_3CHI^+, a daughter ion of CH_3CHI_2) at 308.4 nm. The x-axis is the laser pulse energy, which is proportional to the laser fluence. The lines are fits to Eq. (1). (Top inset) Arrival time profiles of CH_3CHOO at different laser fluences at 308.4 nm. (Bottom) Saturation curve for laser depletion of CH_3CHOO ($m/z = 60$) at 351.8 nm. The x-axis is the absolute laser fluence, deduced from the laser pulse energy and the measured laser beam profile. The line is the fit to Eq. (1).

However, the unknown temperature effect at 352 nm, which is on the weak tail of the CH_3CHI_2 UV absorption band, may introduce error. This complication was circumvented by measuring the absolute laser fluence I directly, as discussed above. Figure 3 (bottom) shows the CH_3CHOO depletion at different laser fluences and the fit to Eq. (1), from which $\sigma(CH_3CHOO)$ can be determined. In order to compare the CH_3CHOO cross section results from the two methods (i.e., the CH_3CHI_2 reference and the absolute laser fluence methods), the laser intensity profile at 308 nm was also measured and used to determine the absolute CH_3CHOO cross section.

Table I summarizes the laser depletion results for CH_3CHOO at 308 and 352 nm as well as for CH_2OO at 352 nm. These absolute cross sections are also plotted in Figure 2. The CH_3CHOO spectra obtained with the methods outlined above were scaled to the average cross section at 308 nm obtained from laser depletion. Here, we assume the temperature effect on the cross sections of CH_3CHOO is negligible at 308 nm. This assumption is reasonable since 308 and 352 nm are near the peak of the UV absorption band, as in the case of CH_2OO.[13] For both CH_3CHOO and CH_2OO, the scaled room-temperature cross sections at 352 nm are

TABLE I. Absolute absorption cross sections of CH_3CHOO and CH_2OO measured by laser depletion in a jet-cooled molecular beam.

Molecule	Wavelength (nm)	Method	Cross section (cm^2)
CH_3CHOO	308.4	CH_3CHI_2 reference	$(10.9^a \pm 0.9^b) \times 10^{-18}$
		Absolute laser fluence	$(10.3 \pm 0.9^b) \times 10^{-18}$
	351.8	Absolute laser fluence	$(9.7 \pm 0.6^b) \times 10^{-18}$
CH_2OO	351.8	Absolute laser fluence	$(11.0 \pm 0.8^b) \times 10^{-18}$

[a]Calculated using the measured value of 3.85 ± 0.19 for the ratio $\sigma\phi(CH_3CHOO)/\sigma\phi(CH_3CHI_2)$ and $\sigma(CH_3CHI_2) = (2.83 \pm 0.20) \times 10^{-18}$ cm^2 $molecule^{-1}$;[41] $\phi(CH_3CHI_2)$ and $\phi(CH_3CHOO)$ are assumed to be unity. See the supplementary material[25] for error estimation.
[b]1σ uncertainty.

consistent with the absolute cross sections measured in the jet-cooled molecular beams (see Figure 2), further supporting the validity of our assumption that temperature has little effect near the absorption peaks. The peak cross section for CH_3CHOO is $(1.27 \pm 0.11) \times 10^{-17}$ cm^2 $molecule^{-1}$ at 328 nm. Numerical values for the CH_3CHOO absorption cross sections as a function of wavelength can be found in the supplementary material.[25]

The CH_3CHOO spectra obtained in this work are compared in Figure 2 with the CH_2OO spectrum reported by Ting *et al.*[13] The peak wavelength for CH_3CHOO at 328 nm is blue shifted by 14 nm from the CH_2OO peak at 342 nm. Previous theoretical calculations attributed this wavelength shift to stabilization of the ground electronic state and destabilization of the excited electronic state of the *syn*-conformer of CH_3CHOO, which dominates CH_3CHOO populations over the *anti*-conformer at 298 K.[23] This blue shifted spectrum has also been demonstrated by Beames *et al.*[23] for *syn*-CH_3CHOO in comparison with CH_2OO under jet-cooled conditions, although (as discussed below) their uncertainty may be larger.

While clear vibronic structure on the long wavelength side was observed for CH_2OO by Ting *et al.*[13] and by Sheps,[12] the CH_3CHOO absorption shows a similar but much weaker structure (i.e., a step-like oscillation). This smearing of the vibronic structure may be expected for a molecule with more degrees of freedom. There are two possible reasons why the oscillatory structure in the CH_3CHOO spectra (Figure 2, 330–380 nm) appears stronger in the SO_2-scavenging spectrum than in the self-reaction spectrum. We think there are two possible reasons. First, because the SO_2-scavenging spectrum is obtained from the difference between two spectra (with and without SO_2), the noise level in the SO_2-scavenging spectrum is much higher than that in the self-reaction spectrum. Some structure may appear more "oscillatory" when the noise is higher. Second, we cannot rule out the possibility that the oscillatory structure belongs to one of the two stable conformers (*syn* and *anti*) of CH_3CHOO. These two conformers may have different reactivity towards SO_2 and towards themselves, such that the SO_2-scavenging and self-reaction spectra are different in the relative conformer populations.

Measurements of the CH_3CHOO spectrum by Beames *et al.*[23] are also plotted in Figure 2, scaled by a factor of 0.25 to roughly match the 308 nm cross section reported

here for easier comparison. The discrepancies are surprising, especially since both studies used laser depletion in a molecular beam to determine the cross sections. In particular, their scaled cross section value at 352 nm is significantly smaller or, alternatively, their unscaled cross section is significantly larger than our data from 300 to 350 nm. For the earlier CH_2OO studies, the inconsistencies between the CH_2OO laser depletion data from Beames *et al.*[11] and from our group[13] were primarily at wavelengths longer than 352 nm and might therefore be explained by a possible temperature effect around 380 nm.[13] However, such a possibility is ruled out for CH_3CHOO in this work by the use of the absolute laser fluence to determine the cross section of CH_3CHOO in the molecular beam at 352 nm directly. One possible cause of the discrepancies may be that Beames *et al.* only used the beam spot size, not a beam profiler measurement, to deduce their laser fluence,[23] which may have larger uncertainty due to the inhomogeneity in the laser beam.

Isomer interference could also cause the observed discrepancies. Beames *et al.*[23] detected CH_3CHOO with photoionization at 10.5 eV. This method provides isomer selectivity because the ionization energies of *syn*- and *anti*-CH_3CHOO are about 9.4 and 9.3 eV, respectively,[22] and other isomers have higher ionization energies.[22] In this work we used electron impact ionization at 45 eV to detect CH_3CHOO and CH_3CHI_2. Electron impact ionization at 45 eV would not discriminate isomers. To determine the potential impact of isomer interference, we calculated the oscillator strengths of relevant UV transitions for the possible isomers of CH_3CHOO with the CCSD-EOM method.

The results are shown in Table II. The *syn*- and *anti*-CH_3CHOO Criegee intermediates absorb very strongly in the near UV range, while the other isomers acetic acid, dioxirane, bisoxy, etc. absorb either rather weakly or at much shorter wavelengths. Two radical-radical complexes ($CH_3CO\cdots OH$ complex 1 and 2) involving an acetyl radical and an OH radical were also considered. Complex 1 has an absorption peak at 307 nm, but its intensity is much weaker than that for CH_3CHOO. Furthermore, its energy is calculated to be ~12 kcal/mol higher than that for *syn*-CH_3CHOO. Thus, this isomer is not expected to contribute to the measured spectrum. Complex 2 absorbs strongly in the near UV range (345 nm) and is calculated to be 11 kcal mol^{-1} more stable than *syn*-CH_3CHOO. However, our preliminary calculation using B3LYP/aug-cc-pVTZ shows that the isomerization barrier of complex 2 is only 1.55 kcal mol^{-1} (see Figure S11 of the supplementary material[25]). We therefore predict that this complex is highly unstable and would isomerize to more stable isomers before being detected in our experiments (which have a time scale on the order of 1 ms).

TABLE II. Relative energies, E_{rel}, of the possible isomers of CH_3CHOO calculated at the CCSD(T)/aug-cc-pVTZ level, and peak positions, λ_{max}, and oscillator strengths, *f*, of the relevant electronic transitions calculated with CCSD-EOM/aug-cc-pVTZ. Detailed information can be found in the supplementary material.[25]

	E_{rel} (kcal mol^{-1})	λ_{max} (nm)	*f*
syn-CH_3CHOO	0.00	294	1.55×10^{-1}
anti-CH_3CHOO	3.71	322	1.73×10^{-1}
Dioxirane (dioxy)	− 23.30	291	9.88×10^{-4}
bisoxy[a]	− 5.46[a]	281	1.57×10^{-3}
anti-CH_3COOH	− 112.88	208	3.57×10^{-4}
syn-CH_3COOH	− 107.78	212	5.46×10^{-4}
anti-CH_2CHOOH	− 17.43	232	2.25×10^{-2}
syn-CH_2CHOOH	− 18.88	193	2.99×10^{-2}
$CH_3CO\cdots OH$ complex 1	12.17	307	1.23×10^{-2}
$CH_3CO\cdots OH$ complex 2	− 10.72	345	6.03×10^{-1}

[a]Since multireference character is important for this isomer, we were not able to optimize the geometry with the single reference CCSD(T) method. Instead, we used the geometry and energy obtained with CASSCF(16,14)/aug-cc-pVDZ. The listed energy is with respect to the *syn*-CH_3CHOO conformer calculated at the same CASSCF level.

From the above theoretical results, we can conclude that *syn*- and *anti*-CH_3CHOO are the main carriers of the observed absorption spectrum, with *anti*-CH_3CHOO absorbing at longer wavelengths. Taatjes *et al.* inferred from their PIMS investigation that syn-CH_3CHOO is dominant (90% in population) at 298 K,[22] which is also consistent with our theoretical calculation. Considering the above discussion, the temperature effect should be minor at 308 and 352 nm wavelengths, which are near the absorption peak at 328 nm. Still, there may be subtle differences between the absorption of CH_3CHOO at room temperature and in a jet-cooled molecular beam. First, in the jet-cooled molecular beam of CH_3CHOO, it might be expected that the *anti*-conformer has an even smaller population than in room temperature CH_3CHOO. However, the barrier to interconversion of these conformers is about 38 kcal mol^{-1}.[45] Because of this high barrier, the rapid cooling process in the supersonic expansion would not reach thermal equilibrium, resulting in similar conformer populations as before expansion. Second, CH_3CHOO has low frequency vibrational modes which could be effectively cooled by the supersonic expansion in a molecular beam. As a result, there would be more hot bands in a room-temperature spectrum than in a jet-cooled spectrum. This may partly explain the longer wavelength tail in our UV spectrum at 295 K as compared to the jet-cooled spectrum reported by Beames *et al.*[23]

With regard to the role of CH_3CHOO in atmospheric photochemistry, we can calculate its photolysis rate coefficients (*J*-values) based on the absorption spectrum obtained in this work and its convolution with the solar flux.[46] A comparison of photolysis lifetimes (i.e., $\tau = J^{-1}$) in the supplementary material[25] shows that a somewhat longer photolysis lifetime is expected for CH_3CHOO relative to CH_2OO (~7 and ~6 s, respectively, at a solar zenith angle (SZA) of 0°; 169 and 132 s, respectively, at 86° SZA). The difference results from the fact that, although the peak cross section for CH_3CHOO of 1.27×10^{-17} cm^2 is similar to that for CH_2OO (1.23×10^{-17} cm^2 reported by Ting *et al.*),[13] the blue shift of the CH_3CHOO spectrum reduces overlap with the solar flux at earth's surface. Although the blue shifted spectrum and reduced overlap with the solar flux for CH_3CHOO versus CH_2OO have been reported previously in Ref. 23 for jet-cooled CH_3CHOO, the quantitative cross sections and spectral shapes are different for this work versus those reported in Ref. 23, resulting in significantly different photolysis lifetimes. As shown in the supplementary material,[25] the more intense but narrower absorption band of CH_3CHOO reported by Beames *et al.*[23] results in shorter photolysis lifetimes (65%−91% of our values,

depending on the solar zenith angle). Similarly, the cross sections of CH_2OO reported by the same group[11] results in a photolysis lifetime of 2.5 s at 0° SZA which is shorter than the corresponding value of 6 s based on the cross sections of our group.[13]

CH_3CHOO reacts quickly with atmospheric gases like SO_2, NO_2, and H_2O.[22] Based on the reported rate constants,[22] the reactive lifetime is shorter than its photolysis lifetime in typical atmospheric conditions, making its photolysis a minor process in the atmosphere.

SUMMARY

The CH_3CHOO UV absorption spectrum was measured by transient absorption spectroscopy, and absolute absorption cross sections were determined at 308 and 352 nm by laser depletion. In the transient absorption measurements, SO_2 scavenging and self-reaction of CH_3CHOO were used to extract the spectrum of CH_3CHOO. In the laser depletion experiments, two methods were used to calibrate the laser fluence: CH_3CHI_2 as a reference molecule and a laser beam profiler measurement. The cross sections presented here may facilitate analysis of the impact of CH_3CHOO photolysis in the atmosphere, and may also provide a useful spectral signature for detection of this Criegee intermediate in laboratory investigations.

ACKNOWLEDGMENTS

This work was supported by Academia Sinica and Ministry of Science and Technology, Taiwan (NSC100-2113-M-001-008-MY3 (J.J.L.), NSC102-2113-M-001-012-MY3 (K.T.)). The authors thank Professor Yuan T. Lee for discussions.

[1] W. H. Bunnelle, Chem. Rev. **91**, 335–362 (1991).
[2] C. A. Taatjes, D. E. Shallcross, and C. J. Percival, Phys. Chem. Chem. Phys. **16**, 1704–1718 (2014).
[3] R. Criegee, Angew. Chem., Int. Ed. **14**, 745–752 (1975).
[4] R. Criegee and G. Wenner, Liebigs Ann. Chem. **564**, 9–15 (1949).
[5] M. Olzmann, E. Kraka, D. Cremer, R. Gutbrod, and S. Andersson, J. Phys. Chem. A **101**, 9421–9429 (1997).
[6] J. H. Kroll, S. R. Sahay, J. G. Anderson, K. L. Demerjian, and N. M. Donahue, J. Phys. Chem. A **105**, 4446–4457 (2001).
[7] C. A. Taatjes, G. Meloni, T. M. Selby, A. J. Trevitt, D. L. Osborn, C. J. Percival, and D. E. Shallcross, J. Am. Chem. Soc. **130**, 11883–11885 (2008).
[8] O. Welz, J. D. Savee, D. L. Osborn, S. S. Vasu, C. J. Percival, D. E. Shallcross, and C. A. Taatjes, Science **335**, 204–207 (2012).
[9] Y.-T. Su, Y.-H. Huang, H. A. Witek, and Y.-P. Lee, Science **340**, 174–176 (2013).
[10] M. Nakajima and Y. Endo, J. Chem. Phys. **139**, 101103 (2013).
[11] J. M. Beames, F. Liu, L. Lu, and M. I. Lester, J. Am. Chem. Soc. **134**, 20045–20048 (2012).
[12] L. Sheps, J. Phys. Chem. Lett. **4**, 4201–4205 (2013).
[13] W.-L. Ting, Y.-H. Chen, W. Chao, M. C. Smith, and J. J.-M. Lin, Phys. Chem. Chem. Phys. **16**, 10438–10443 (2014).
[14] J. H. Lehman, H. Li, J. M. Beames, and M. I. Lester, J. Chem. Phys. **139**, 141103 (2013).
[15] B. Ouyang, M. W. McLeod, R. L. Jones, and W. J. Bloss, Phys. Chem. Chem. Phys. **15**, 17070–17075 (2013).
[16] Z. J. Buras, R. M. I. Elsamra, A. Jalan, J. E. Middaugh, and W. H. Green, J. Phys. Chem. A **118**, 1997–2006 (2014).
[17] D. Stone, M. Blitz, L. Daubney, N. U. M. Howes, and P. Seakins, Phys. Chem. Chem. Phys. **16**, 1139–1149 (2014).
[18] Y. Liu, K. D. Bayes, and S. P. Sander, J. Phys. Chem. A **118**, 741–747 (2014).
[19] O. Welz, A. J. Eskola, L. Sheps, B. Rotavera, J. D. Savee, A. M. Scheer, D. L. Osborn, D. Lowe, A. M. Booth, P. Xiao, M. A. H. Khan, C. J. Percival, D. E. Shallcross, and C. A. Taatjes, Angew. Chem. **126**, 4635–4638 (2014).
[20] Y.-T. Su, H.-Y. Lin, R. Putikam, H. Matsui, M. C. Lin, and Y.-P. Lee, Nature Chemistry **6**, 477–483 (2014).
[21] M. Boy, D. Mogensen, S. Smolander, L. Zhou, T. Nieminen, P. Paasonen, C. Plass-Dülmer, M. Sipilä, T. Petäjä, L. Mauldin, H. Berresheim, and M. Kulmala, Atmos. Chem. Phys. **13**, 3865–3879 (2013).
[22] C. A. Taatjes, O. Welz, A. J. Eskola, J. D. Savee, A. M. Scheer, D. E. Schallcross, B. Rotavera, E. P. F. Lee, J. M. Dyke, D. K. W. Mok, D. L. Osborn, and C. J. Percival, Science **340**, 177–180 (2013).
[23] J. M. Beames, F. Liu, L. Lu, and M. I. Lester, J. Chem. Phys. **138**, 244307 (2013).
[24] M.-N. Su and J. J.-M. Lin, Rev. Sci. Instrum. **84**, 086106 (2013).
[25] See supplementary material at http://dx.doi.org/10.1063/1.4892582 for details.
[26] C. Lee, W. Yang, and R. G. Parr, Phys. Rev. B **37**, 785 (1988).
[27] A. D. Becke, J. Chem. Phys. **98**, 5648 (1993).
[28] R. J. Bartlett and G. D. Purvis III, Int. J. Quantum Chem. **14**, 561–581 (1978).
[29] J. A. Pople, R. Krishnan, H. B. Schlegel, and J. S. Binkley, Int. J. Quantum Chem. **14**, 545–560 (1978).
[30] G. D. Purvis III and R. J. Bartlett, J. Chem. Phys. **76**, 1910–1918 (1982).
[31] J. A. Pople, M. Head-Gordon, and K. Raghavachari, J. Chem. Phys. **87**, 5968–5975 (1987).
[32] H.-J. Werner and P. J. Knowles, J. Chem. Phys. **82**, 5053 (1985).
[33] P. J. Knowles and H.-J. Werner, Chem. Phys. Lett. **115**, 259 (1985).
[34] T. H. Dunning, Jr., J. Chem. Phys. **90**, 1007–1023 (1989).
[35] R. A. Kendall, T. H. Dunning, Jr., and R. J. Harrison, J. Chem. Phys. **96**, 6796–6806 (1992).
[36] H. Koch and P. Jørgensen, J. Chem. Phys. **93**, 3333–3344 (1990).
[37] J. F. Stanton and R. J. Bartlett, J. Chem. Phys. **98**, 7029–7039 (1993).
[38] H. Koch, R. Kobayashi, A. S. d. Merás, and P. Jørgensen, J. Chem. Phys. **100**, 4393–4400 (1994).
[39] M. J. Frisch, G. W. Trucks, H. B. Schlegel *et al.*, Gaussian 09, Revision A.02, Gaussian, Inc., Wallingford, CT, 2009).
[40] H.-J. Werner, P. J. Knowles, F. R. Manby, M. Schutz *et al.*, MOLPRO, version 2010.1, a package of *ab initio* programs, 2010, see http://www.molpro.net.
[41] S. P. Sander, J. Abbatt, J. R. Barker, J. B. Burkholder, R. R. Friedl, D. M. Golden, R. E. Huie, C. E. Kolb, M. J. Kurylo, G. K. Moortgat, V. L. Orkin, and P. H. Wine, "Chemical kinetics and photochemical data for use in atmospheric studies, Evaluation No. 17," JPL Publication 10-6 (Jet Propulsion Laboratory, Pasadena, 2011), see http://jpldataeval.jpl.nasa.gov.
[42] J. J.-M. Lin, D. W. Hwang, S. Harich, Y. T. Lee, and X. Yang, Rev. Sci. Instrum. **69**, 1642–1646 (1998).
[43] H.-Y. Chen, C.-Y. Lien, W.-Y. Lin, Y. T. Lee, and J. J.-M. Lin, Science **324**, 781–784 (2009).
[44] J. C. Mossinger, D. E. Shallcross, and R. A. Cox, J. Chem. Soc. Faraday Trans. **94**, 1391–1396 (1998).
[45] K. T. Kuwata, M. R. Hermes, M. J. Carlson, and C. K. Zogg, J. Phys. Chem. A **114**, 9192 (2010).
[46] B. J. Finlayson-Pitts and J. N. Pitts, *Chemistry of the Upper and Lower Atmosphere* (Academic Press, San Diego, 2000).